JOURNAL OF CHEMICAL INFORMATION AND MODELING

Article

pubs.acs.org/jcim

Toward an Optimal Docking and Free Energy Calculation Scheme in Ligand Design with Application to COX-1 Inhibitors

Yasmin Shamsudin Khan, Hugo Gutiérrez-de-Terán, Lars Boukharta, and Johan Åqvist*

Department of Cell and Molecular Biology, Box 596, Uppsala University, BMC, SE-751 24 Uppsala, Sweden

Supporting Information

ABSTRACT: Cyclooxygenase-1 (COX-1) is one of the main targets of most pain-relieving pharmaceuticals. Although the enzyme is well characterized, it is known to be a difficult target for automated molecular docking and scoring. We collected from the literature a structurally diverse set of 45 nonsteroidal anti-inflammatory drugs (NSAIDs) and COX-2-selective inhibitors (coxibs) with a wide range of binding affinities for COX-1. The binding of this data set to a homology model of human COX-1 was analyzed with different combinations of molecular docking algorithms, scoring functions, and the linear interaction energy (LIE) method for estimating binding affinities. It is found that the computational protocols for estimation of binding affinities are extremely sensitive to the initial orientations of the ligands in the binding pocket. To overcome this limitation, we propose a systematic exploration of docking poses using the LIE calculations as a postscoring function. This scheme yields predictions in excellent agreement with experiment, with a mean unsigned error of 0.9 kcal/mol for binding free energies and structures of high quality. A significant improvement of the results is also seen when averaging over experimental data from several independent measurements.

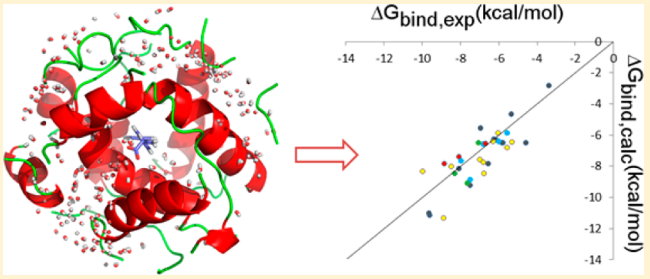

INTRODUCTION

Nonsteroidal inflammatory drugs (NSAIDs) are widely used to treat musculoskeletal and arthritic symptoms as well as for reducing common fevers and for pain relief. In 2009, NSAIDs, including the subclass of selective COX-2 inhibitors, represented 35% of the market share by sales of pain relieving pharmaceuticals.[1] However, it is well recognized that there is low awareness of their side effects,[2] which for traditional NSAIDs include kidney problems,[3,4] gastric intestinal bleeding, and formation of peptic ulcers.[5] These effects are related to poor selectivity in their mechanism of action, which is the inhibition of the enzyme prostaglandin H_2-synthase, often referred to as cyclooxygenase (COX). Three isoforms exist, namely COX-1,[6] COX-2,[7] and COX-3[8] (also known as COX-1b), which are responsible for the production of prostaglandins (PG) from arachidonic acid (AA). This is achieved by catalysis of (i) conversion of AA into prostaglandin G2, which occurs at the so-called COX site, and (ii) the reduction of PGG2 to prostaglandin H2 at the peroxidase site of the COX enzyme, with the participation of the heme group as electron donator. Among the different PGs produced, PGE_2 causes pain sensitization and the thromboxanes are responsible for blood clotting (thrombosis). The COXs are homodimers that exhibit half-of-sites COX activity, meaning that only one protomer in the dimer unit is catalytically active at a time, while the other acts as an allosteric subunit.[9] Inhibitors bind to the COX site and crystal structures generally show occupancy of both COX sites in the dimer.

The COX-2 isoform is induced during inflammation,[10] and it is widely believed that inhibition of this isoform is responsible for the pain inhibition of NSAIDs, whereas inhibition of COX-1, the constitutive isoform with housekeeping functions present in most tissues and blood cells, also causes several adverse side effects. Following this line of thinking, considerable efforts were made at formulating COX-2 selective NSAIDs, popularly known as coxibs. Such drugs were successfully launched to the market, although many were withdrawn a few years later due to strong side effects, such as the increased risks of cardiac failure due to blood clotting in the heart (myocardial infarction).[11−13] Thus, inhibition of COX-1 and its subsequent prevention of thromboxane formation might have a heart protection effect that counterbalances inhibition of COX-2. It follows that COX-1 is still of interest when designing new anti-inflammatory, analgesic and antipyretic drugs, a line of thinking that was reinforced by the recently discovered COX-1 selective inhibitors displaying analgesic effects while free of gastric ulcer formation.[14] A balanced binding profile to both enzymes seems to be the optimal solution to minimize side effects of novel analgesics, following the paradigm of polypharmacology.[15]

Since experimental binding assay measurements for candidate inhibitors to the different targets (and antitargets) are time-consuming and expensive, computational solutions where large databases of compounds are screened in silico against a battery of proteins are valuable, in particular if

Received: March 10, 2014
Published: April 30, 2014

dx.doi.org/10.1021/ci500151f | J. Chem. Inf. Model. 2014, 54, 1488−1499

accurate predictions of binding affinities can be provided. Automated molecular docking is one of the most popular methods for virtual screening. Here, binding affinity estimations are given as "scores" based on statistical or force-field based scoring functions. However, the developers of one of the most popular docking algorithms (DOCK)[16] showed how difficult it was to distinguish between decoys and true hits in the case of COX-1.[17] Other experimental and computational studies on the COX systems include docking studies to determine the pharmacophores of various ligand classes,[18] NMR studies,[19] molecular dynamics (MD) simulations for evaluating the binding modes of various substrates in COX-1 and COX-2,[20−22] and Monte Carlo simulations in combination with the extended linear response approach to estimate binding affinities for a class of COX-2 ligands.[23] It is clear that with increasing computer power more accurate estimations of binding affinities can be incorporated into the virtual screening workflow.

The linear interaction energy (LIE) method is a widely used technique for estimating binding affinities in various systems, such as enzymes[24−27] and ion channels.[28,29] Here, energies are computed from appropriate sampling by MD or Monte Carlo simulations of the ligand in its relevant biophysical states, i.e., bound to the enzyme or free in solution (reference state). Additional advantages of methods like LIE over simplified scoring functions include the explicit consideration of water-mediated interactions, which are often lacking in docking algorithms, the identification of key residues in modulation of ligand affinities, and the explicit consideration of the solvated reference state of the ligand. In the aforementioned ligand design applications of the LIE method, the ligand series examined often shared a common scaffold, which is a clear advantage in the elucidation of a common binding mode and the establishment of initial structure-affinity relationships. In this sense, the case of NSAIDs is particularly challenging given the considerable diversity in chemical structure of different inhibitors, with several scaffolds achieving a wide range of affinities for the COX-1 target. Consequently, an optimized computational protocol, combining molecular docking and LIE based binding affinity calculations, would be very useful for analysis of binding modes and structure-affinity relationships of a diverse set of traditional NSAIDs and coxibs as COX-1 inhibitors. In contrast, in more simple cases where only one chemical scaffold is investigated, one often finds that a fully automated protocol is not advisible, but that expert manual supervision is needed. Herein, we develop an optimized scheme, which combines automated and manual docking with the LIE methodology used as a postscoring function with default parameters. It achieves excellent agreement with experimental results allowing the establishment of previously unobserved structure−activity relationships. The scheme is clearly transferable to other systems and is expected to be useful in the lead-optimization phase of any drug design project.

MATERIAL AND METHODS

Homology Modeling and Molecular Docking. The human COX-1 structure was generated on the basis of the highly similar ovine COX-1 with 91% sequence identity (PDB code 1Q4G)[30] using default homology modeling routines in Modeller.[31] The heme group was imported from the crystal structure by structural superposition. The resulting structure was used as input for ligand docking using two different docking programs, GLIDE[32] and GOLD.[33] Addition of protons was done with the corresponding algorithms implemented in the different docking programs. The docking search was centered in all cases on the position equivalent to the atom C12 in the inhibitor BFL cocrystallized with the template 1Q4G (Figure 1). In GLIDE (version 5.8), the considered search

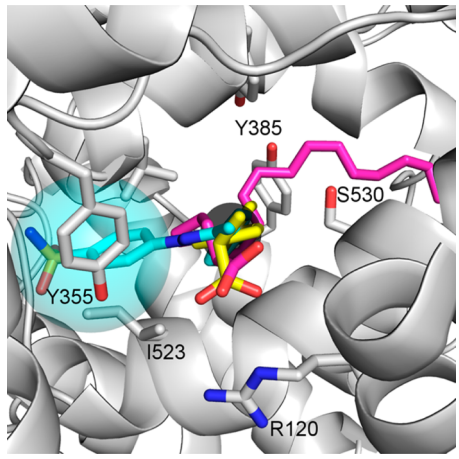

Figure 1. Detailed view of the binding site of the hCOX-1 model with the natural substrate arachidonic acid (magenta),[69] the inhibitor BFL (yellow)[30] and the selective COX-2 inhibitor celecoxib (cyan)[71] superimposed from their respective crystal structures. The side pocket and the center point of the regions used for molecular docking and MD simulations are highlighted as blue and black spheres, respectively.

volume was confined within a cube of 20 Å^3. 5000 poses per ligand were kept for the initial phase of docking and the best 400 poses per ligand were kept for energy minimization. In GOLD (version 5.1) the search was confined within a sphere of 10 Å radius around the center defined above, with the slowest and most accurate genetic algorithm search options and generating 10 poses per ligand. All four built-in scoring functions in GOLD (ChemPLP, GoldScore, ChemScore, and ASP) were used in parallel docking explorations. Finally, manual docking was performed in selected cases using the PyMOL[34] graphical interface. All ligand structures were built using the software Maestro[35] included in the Schrödinger Suite 2011 package and energy minimized using Macromodel[36] with the OPLS_2005 force field. Carboxylated ligands were modeled as negatively charged, and for the enantiomeric compounds both isoforms were built.

MD Simulations. MD simulations were performed using the program Q[37] with the OPLS-AA force field.[38] The parameters needed for the ligands that were not present in the original version of the force field were retrieved from automatic parametrization performed with Macromodel.[36] Spherical boundary conditions were used, with a simulation sphere of 20 Å radius centered on the same point as defined for the docking calculations. This sphere was solvated with TIP3P[39] water molecules and subject to polarization and radial constraints according to the surface constrained all-atom solvent (SCAAS) model[37,40] at the sphere surface, to mimic the properties of bulk water. Nonbonded interactions were calculated explicitly up to a 10 Å cutoff, except for the ligand atoms for which no cutoff was used. Beyond the cutoff, long-range electrostatics were treated with the local reaction field multipole expansion method.[41] All solvent bonds and angles were constrained with the SHAKE[42] algorithm and a 1 fs MD time step size was used. The MD simulations were carried out at a temperature of 298 K. Nonbonded pair lists were updated

dx.doi.org/10.1021/ci500151f | J. Chem. Inf. Model. 2014, 54, 1488−1499

every 25 steps and the same interval was used for the sampling of the ligand-surrounding interaction energies. The convergence was estimated by dividing the whole trajectory into two halves of equal length and the associated errors were estimated as the difference between the average energies of the first and second half of the data collection phase.

Each ligand−protein docking pose was subjected to five independent MD simulations using the same conditions but with different initial random velocities. Protein atoms outside the simulation sphere were restrained to their initial positions and only interacted with the system through bonds, angles, and torsions. The ionization states of titratable residues inside the simulation sphere were manually assessed with the following residues treated as ionized: Asp190, Glu520, Glu524, Arg120, His90, and His513. Ionizable residues within 5 Å of the sphere boundary were modeled in their neutral form to account for dielectric screening, as well as those outside the simulation sphere. With this setup the simulation sphere was overall neutral, except for the charge of ligands bearing a carboxylate group. Hence the protein and water (reference) simulation systems have the same net charge, which avoids the consideration of additional Born terms in the calculation of free energies. The equilibration phase lasted for 0.5 ns, during which all solute heavy atoms were restrained and gradually released as the temperature increased. No restraints were applied during the final 140 ps, preceding the subsequent data collection phase that lasted for 2.5 to 5 ns, depending on the convergence achieved. It may be noted here that the average convergence error for the estimated binding free energies is only ±0.53 kcal/mol (cf. Table 3). Likewise, each ligand was subjected to five independent MD simulations in water following the same scheme but with different initial random velocities. After a similar equilibration scheme, this was followed by a 1 ns unrestrained MD production phase, where a weak harmonic restraint (10 kcal/mol·Å^2) was applied to the center of mass of the ligand.

There are clear advantages with performing MD simulations using the spherical boundary conditions implemented in Q,[37] which have been specifically designed to enable extensive and efficient free energy perturbation and LIE calculations. That is, not only is the size of the system reduced, but possible larger scale conformational fluctuations distal to the binding site, which may require much longer time scales for convergence, are avoided. In this respect, reduced spherical models that still yield correct structural fluctuations of the binding site[43] may be significantly more efficient than more standard large periodic boundary models, precisely because they do not sample such long time scale motions. In the COX homodimer case, single binding site simulations are likely to yield a more reliable description of the ligand binding energetics since no long time scale communication between monomers is considered.

Binding Affinity Calculations. Binding free energies were calculated using the linear interaction energy (LIE) method.[44,45] Here, binding affinities (ΔG^{calc}_{bind}) are estimated on the basis of the difference (Δ) in average ligand−surrounding interaction energies $\langle U_{l-s}\rangle$ extracted from the MD simulations of the ligand in the two states referred to above, i.e. in water and embedded in the active site of the solvated protein, respectively. The nonpolar $\langle U^{vdW}_{l-s}\rangle$ and polar $\langle U^{el}_{l-s}\rangle$ interaction energies are treated separately, and their difference is scaled by different scaling factors, α and β:

$$\Delta G^{calc}_{bind} = \alpha\Delta\langle U^{vdW}_{l-s}\rangle + \beta\Delta\langle U^{el}_{l-s}\rangle + \gamma \quad (1)$$

The constant α has been empirically set to 0.18 while β varies depending on the properties of the ligand.[45,46] In our case, the value of β is 0.33 for neutral ligands with two or more hydroxyl groups, 0.37 for neutral ligands with one hydroxyl group, 0.43 for all remaining neutral ligands, and 0.5 for all ligands bearing a negatively charged carboxylate group. Unlike α and β, the parameter γ generally depends on the protein binding site (its hydrophobicity or desolvation cost)[47] and was treated as a free parameter and empirically adjusted. An electrostatic correction term[48] ΔG^{el}_{corr} was calculated for the interactions of charged ligands with distant neglected ionized groups that were neutralized in the simulations, as follows (kcal/mol)

$$\Delta G^{el}_{corr} = 332 \sum_p \sum_l \frac{q_p q_l}{\varepsilon r_{pl}} \quad (2)$$

where q_p is the formal charge of the neglected ionic group while q_l is the partial charge of the ligand atom and the effective dielectric constant ε was set to 80. The offset parameter γ was optimized to minimize the absolute error between calculated and experimental binding free energies and initially this optimization was only based on ligands with known crystallographic binding mode (it does not affect relative binding free energies). Experimental binding free energies (ΔG^{exp}_{bind}) were calculated from IC_{50} values as

$$\Delta G^{exp}_{bind} = RT\ln K_d = RT\ \ln IC_{50} + c \quad (3)$$

where c is an assay-specific constant that depends on the substrate concentration and the enzymatic K_M value.[49] Since c is constant for a given assay it will be implicitly included in the optimized γ of eq 1.

Statistical Analyses. The diversity of the ligand data set was assessed by a pairwise comparison of all compounds on the basis of the extended-connectivity fingerprints (ECFPs).[50] Briefly, ECFPs are topological circular fingerprints explicitly designed to capture molecular features relevant to molecular activity, and were in this case calculated with the GenerateMD tool implemented in JChem.[51] The Tanimoto diversity coefficient was calculated for each molecule pair A and B using the equation

$$T(A, B) = 1 - \frac{N_{A\cap B}}{N_A + N_B - N_{A\cap B}} \quad (4)$$

where N_A represents the number of bits present in the fingerprint of structure A, N_B represents the number of bits present in the fingerprint of structure B, and $N_{A\cap B}$ represents the number of bits common to both fingerprints of structures A and B. The resulting coefficient T(A, B) ranges between 0 and 1 where 0 indicates very high similarity and 1 complete dissimilarity.

The Pearson correlation coefficient r was used to assess the performance of the different scoring functions and the LIE method, according to the equation

$$r = \frac{\sum (x_i - \overline{x}_i)(y_i - \overline{y}_i)}{\sqrt{\sum (x_i - \overline{x}_i)^2 \sum (y_i - \overline{y}_i)^2}} \quad (5)$$

where x_i refers to the observed experimental values (ΔG^{exp}_{bind}) and y_i to the calculated values (ΔG^{calc}_{bind}) while $\overline{x}_i$ and $\overline{y}_i$ represent the corresponding mean values. An advantage of r values as compared to the frequently used R^2 value (which accounts for the fraction of the variance explained by the model relative to

the total variance) is that it allows the detection of negative correlations with ΔG^{exp}_{bind} values, even if the correct correlation is positive. It should, however, be noted that the four scoring functions ChemPLP, GoldScore, ChemScore, and ASP all have higher scores for more negative binding free energies, so that the correct correlation in these cases is negative.

RESULTS AND DISCUSSION

Although the crystal structure of COX-1 from sheep has been available since 1994[6] the human COX-1 (hCOX-1) has not yet been crystallized. The generated homology model of hCOX-1 strongly resembles the structure of the sheep ortholog used as a template, which was expected due to their high sequence similarity (91% identity). The Ramachandran plot showed good stereochemical quality, with 94% of nonproline non-glycine residues in the most favored regions and the remaining 6% in additional allowed regions (the corresponding values for the template crystal structure are 90% and 10%, respectively). The structural differences between human and ovine COX-1 are confined to the protein surface, which reinforces the impression that the homology model could be used as a high-quality structure of hCOX-1 for both molecular docking and molecular dynamics simulations.

The ligand data set compiled by Warner and co-workers[52] used in this study consisted of 45 traditional NSAIDs and coxibs. Most of the compounds are or have been available on the market either as "over the counter" or as prescription drugs. The data set is highly diverse in both affinity range and chemical structure (Figure S1, Supporting Information). The calculated Tanimoto diversity index is 0.81, indicative of an overall large structural diversity. More than half (26) of the ligands have a carboxyl group, similar to the natural substrate arachidonic acid (Figure 1). These were modeled in their predominant negatively charged state. Some of these carboxylated ligands are derivatives of 2-arylpropionic acid, which has a chiral center, but the corresponding experimental data refers to the racemic mix. However, it is well-known that 2-arylpropionic acid derivatives are subject to chiral inversions from the *R*-enantiomer to its biologically active *S*-enantiomer in biological systems[53,54] and in vitro.[55] Preliminary parallel simulations of both enantiomers fully agree with this idea, since the *S*-form is consistently revealed as the most potent enantiomer in all cases. Accordingly, the data reported herein is exclusively based on the simulations of the *S*-enantiomers.

Finally, the remaining noncarboxylated ligands in the series correspond to 19 structurally diverse neutral compounds. Although the Warner data set here considered is one of the largest compound sets of NSAIDs examined in a single assay, several other laboratories[56−61] have reported hCOX-1 affinity data for smaller subsets of the compounds included in the Warner set. Most of the compounds that have been examined in several assays show a considerable variance in the reported experimental affinity values, although there are also several cases with very small (<1 kcal/mol) variance (Supporting Information Figure S1). Overall, the experimental IC_{50}-values span between 0.00019 and 4956 μM (corresponding to binding free energies of about −13.2 to −3.1 kcal/mol). However, for seven low affinity ligands the experimental value is reported as IC_{50} > 100 μM. In these cases, we approximated the value IC_{50} = 100 μM as the experimental reference affinity in order to estimate calculated vs. experimental values. However, these compounds were not considered for the estimation of statistical parameters.

LIE Model. The standard LIE parametrization assigns values of α = 0.18 for all ligands, while the value for the electrostatic weight factor (β) varies depending on the chemical nature of the ligand.[45] The value of β is 0.5 for all carboxylated ligands, following the linear response approximation for ligands bearing a net charge. For the rest of the compounds in the data set, this parameter takes a lower value to account for deviations from linear response. In particular, β = 0.43 for neutral compounds without hydroxyl groups, β = 0.37 for neutral compounds with one hydroxyl group and β = 0.33 for compounds with two or more hydroxyl groups. Charged ligands are also subjected to an electrostatic correction term, which accounts for their interactions with distant neutralized ionizable residues. In the present system this term takes the value of ΔG^{el}_{corr} = −1.11 kcal/mol and it, in fact, significantly improves the ranking of charged versus neutral compounds (see below). Finally, the offset parameter γ was empirically adjusted in order to achieve the best fitting between calculated and experimental affinities. This was first done by just considering the small subset of compounds with available X-ray structures and comparing these to the lowest energy modeled conformation (Table 1)

Table 1. Relevant Crystal Structures of COX Complexes

ligand	X-ray	RMSD[a]	$\Delta\Delta G^{(calc-exp)}_{bind}$[b]
celecoxib	3KK6	0.62	1.7
flurbiprofen	2AYL	0.70	−1.5
ibuprofen	1EQG	1.44	0.6
naproxen	3NT1[c]	1.88	−1.4
nimesulide	3N8X	1.79	0.3
salicylic acid	1PTH	1.12	−1.7
diclofenac[e]	3N8Y	5.98	2.0
6MNA	3NT1[c,d]	0.57	0.7
indometacine[e]	2OYE[d]	0.74	4.0
suprofen	1PGE[d]	1.19	0.1

[a]Root mean square ligand coordinate deviation between the lowest energy average MD structure and the crystal structure. [b]Values in kilocalories per mole. [c]Structure determined with COX-2. [d]Crystal structures with substituted functional groups on the cocrystallized inhibitors. [e]Not used in the parametrization of γ.

yielding an optimized value of γ = −6.5 kcal/mol. It is noteworthy that this value did not change significantly (γ = −6.4 kcal/mol) when the whole data set of 45 compounds was included in the final parametrization (Schemes 3 and 4 below), which supports the robustness of the LIE model. As expected, the γ parameter assumes a negative value, indicative of a hydrophobic binding site,[47,62] since the COX enzymes have several aromatic residues in the binding crevice.

Different computational schemes were evaluated for their accuracy in the estimation of the binding affinities for the data set of hCOX-1 inhibitors presented above. The schemes combined automated docking and scoring, MD/LIE rescoring of binding affinities, and different levels of user intervention, as summarized in Figure 2. The different schemes and their associated results are presented below in increasing levels of complexity.

Scheme 1. In Scheme 1, the first stage encompassed automated docking and scoring with six parallel protocols, each of them making use of one scoring function included in the docking programs GOLD and GLIDE. The top pose was selected for every scoring function, and the correlation between the scoring function and the experimental affinity was

dx.doi.org/10.1021/ci500151f | J. Chem. Inf. Model. 2014, 54, 1488−1499

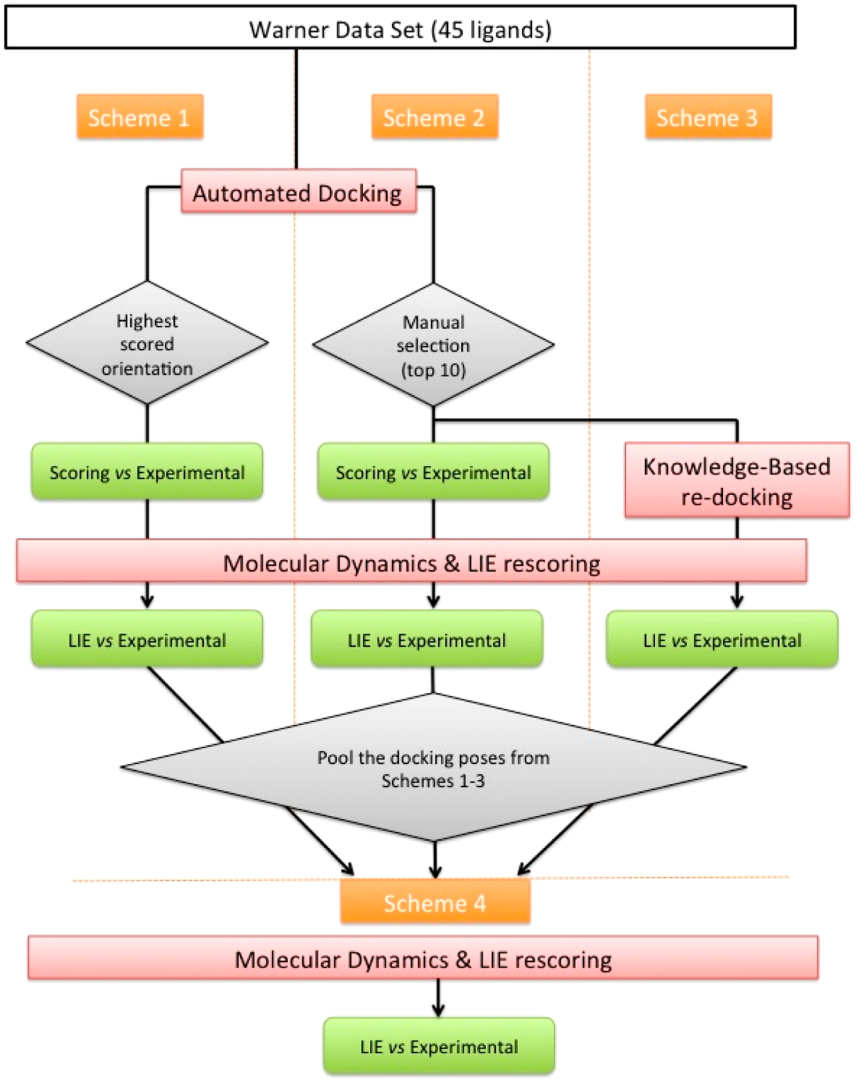

Figure 2. Flowchart depicting the different computational schemes discussed in the text for the calculation of binding free energies.

Table 2. Statistical Quality Measures for the Different Schemes

scheme	scoring function	salt-bridge[a]	r_{score}[b]	±2 kcal/mol[d]	<lerrl>[d]	r_{LIE}[b,d]
Scheme 1	ASP	42%	−0.23	11%	9.50	0.07
	ChemScore	65%	−0.32	26%	7.01	0.20
	GoldScore	77%	−0.35	32%	5.93	0.22
	ChemPLP	73%	−0.39	29%	5.83	0.35
	GlideScore SP	88%	0.30	21%	5.49	−0.12
	GlideScore XP	65%	0.14	24%	8.55	−0.10
Scheme 2	ASP	77%	−0.25	18%	6.62	−0.12
	ChemScore	100%	−0.30	29%	3.99	0.29
	GoldScore	100%	−0.41	37%	4.39	0.01
	ChemPLP	96%	−0.42	37%	3.70	0.19
Scheme 3		100%		63% (69%)	2.06 (1.75)	0.39 (0.55)
Scheme 4		100%		92% (100%)	1.36 (1.01)	0.46 (0.79)
Scheme 4′[e]		100%		89% (97%)	1.11 (0.88)	0.61 (0.81)

[a]Percentage of carboxylated ligands in the salt-bridge docking orientation. [b]The Pearson correlation coefficient for scoring functions (r_{score}) and LIE calculations (r_{LIE}). [c]Percentage of ligands with LIE ΔG^{calc}_{bind} values within 2 kcal/mol of ΔG^{exp}_{bind}. [d]Values in parentheses refer to the statistics after elimination of the outliers indometacine, ketorolac, and zomepirac discussed in the text. [e]Statistics resulting from comparisons with average experimental affinities from different assays.[49,53−58]

independently analyzed. As we show in Table 2, none of the scoring functions provided reliable predictions for the relative experimental affinities, with absolute values for the correlation coefficients (r_{score}) between 0.1 and 0.4 (note again, that a negative correlation is expected for ASP, ChemScore, GoldScore, and ChemPLP). At the second stage, we accepted the

dx.doi.org/10.1021/ci500151f | J. Chem. Inf. Model. 2014, 54, 1488−1499

Table 3. Average Energies from the MD Simulations Yielding the Lowest Predicted Binding Free Energies (kcal/mol)[a]

ligand	$\langle U_{l-s}^{vdW}\rangle_w$			$\langle U_{l-s}^{el}\rangle_w$			$\langle U_{l-s}^{vdW}\rangle_p$			$\langle U_{l-s}^{el}\rangle_p$			$\Delta G_{bind}^{calc\ a,b}$			ΔG_{bind}^{Warner}
6MNA	−11.9	±	0.0	−168.1	±	0.1	−22.9	±	0.2	−162.5	±	0.4	−6.7	±	0.2	−6.0
aspirin	−7.9	±	0.1	−165.2	±	0.1	−14.2	±	0.2	−165.8	±	0.0	−9.0	±	0.1	−7.9
carprofen	−15.3	±	0.3	−171.5	±	0.2	−33.6	±	0.2	−172.0	±	1.2	−11.0	±	0.6	−9.6
diclofenac	−15.9	±	0.1	−170.2	±	0.1	−28.5	±	0.4	−166.0	±	1.7	−7.7	±	0.9	−9.7
fenoprofen	−14.4	±	0.1	−167.0	±	0.4	−26.7	±	0.3	−165.0	±	1.4	−8.7	±	0.7	−7.5
flufenamate	−14.3	±	0.1	−156.6	±	0.4	−24.5	±	0.0	−156.0	±	0.6	−9.1	±	0.4	−7.5
flurbiprofen	−13.7	±	0.2	−161.1	±	0.1	−29.8	±	0.1	−162.7	±	0.4	−11.2	±	0.2	−9.7
ibuprofen	−12.0	±	0.1	−169.6	±	0.2	−25.6	±	0.4	−162.4	±	1.8	−6.4	±	0.9	−7.0
indometacine	−22.7	±	0.0	−170.0	±	0.1	−40.6	±	1.6	−162.0	±	0.8	−6.7	±	0.5	−10.7
ketoprofen	−15.5	±	0.2	−169.2	±	0.4	−32.4	±	1.0	−164.5	±	0.3	−8.2	±	0.3	−10.0
ketorolac	−15.5	±	0.0	−170.1	±	0.0	−32.1	±	1.1	−158.5	±	0.1	−4.7	±	0.2	−13.2
meclofenamate	−16.6	±	0.1	−165.2	±	0.7	−27.3	±	0.5	−162.1	±	0.3	−7.9	±	0.4	−9.1
mefenamic acid	−15.1	±	0.1	−165.0	±	0.4	−26.1	±	0.7	−160.9	±	1.1	−7.4	±	0.6	−6.3
naproxen	−13.4	±	0.0	−167.7	±	1.1	−30.2	±	0.3	−163.4	±	0.5	−8.3	±	0.6	−6.9
niflumic acid	−13.7	±	0.1	−164.2	±	0.1	−24.7	±	0.0	−160.3	±	1.0	−7.5	±	0.5	−6.3
piroxicam	−28.5	±	0.1	−36.1	±	0.3	−45.4	±	2.1	−31.1	±	0.0	−7.3	±	0.4	−7.7
sulindac sulfide	−18.6	±	0.1	−166.7	±	0.6	−39.1	±	1.5	−159.4	±	1.1	−7.5	±	0.7	−7.8
suprofen	−15.7	±	0.1	−170.1	±	1.4	−32.6	±	1.1	−165.0	±	1.3	−8.0	±	1.0	−8.1
tenidap	−26.1	±	0.4	−36.4	±	0.3	−41.9	±	0.2	−40.3	±	0.8	−10.9	±	0.4	−9.7
tolmetin	−15.8	±	0.1	−172.7	±	0.3	−33.1	±	0.4	−168.2	±	1.5	−8.3	±	0.8	−8.8
tomoxiprol	−26.5	±	0.3	−38.5	±	0.1	−44.2	±	0.5	−28.9	±	0.0	−5.4	±	0.1	−7.0
zomepirac	−17.0	±	0.1	−168.7	±	1.1	−36.8	±	0.5	−156.1	±	1.7	−4.7	±	1.0	−8.7
celecoxib	−27.3	±	0.2	−44.5	±	0.9	−53.2	±	0.5	−33.8	±	1.4	−6.4	±	0.7	−8.1
etodolac	−16.9	±	0.1	−181.8	±	0.3	−33.7	±	0.7	−172.2	±	1.1	−5.7	±	0.6	−6.7
meloxicam	−30.7	±	0.2	−26.3	±	0.7	−53.0	±	0.1	−19.8	±	0.5	−7.6	±	0.4	−7.1
nimesulide	−26.2	±	0.2	−30.2	±	0.3	−46.3	±	0.1	−22.0	±	1.7	−6.5	±	0.7	−6.8
NS398	−27.6	±	0.2	−27.4	±	0.5	−48.7	±	1.1	−18.2	±	0.0	−6.3	±	0.3	−7.0
rofecoxib	−27.0	±	0.3	−37.6	±	0.2	−52.7	±	0.7	−25.3	±	0.2	−5.7	±	0.2	−5.7
mesalazine	−3.6	±	0.3	−160.4	±	0.0	−12.5	±	0.7	−154.9	±	1.6	−6.3	±	0.8	−4.6
ampyrone	−19.0	±	0.0	−22.0	±	0.1	−31.0	±	0.8	−16.9	±	1.7	−6.4	±	0.7	−5.8
diflunisal	−11.8	±	0.2	−154.1	±	0.0	−22.5	±	0.4	−144.2	±	1.2	−4.5	±	0.6	−5.4
nabumetone	−23.6	±	0.1	−17.8	±	0.3	−41.1	±	0.4	−10.2	±	0.6	−6.3	±	0.3	−4.5
resveratrol	−15.3	±	0.1	−48.8	±	0.6	−29.8	±	0.0	−42.2	±	0.7	−6.8	±	0.3	−6.2
salicylic acid	−4.1	±	0.0	−151.7	±	0.8	−11.3	±	0.8	−143.7	±	1.5	−4.8	±	0.8	−3.1
sulfasalazine	−25.5	±	0.1	−185.5	±	0.2	−44.7	±	1.0	−168.9	±	3.5	−2.7	±	1.8	−3.4
tamoxifen	−34.8	±	0.6	−19.6	±	0.1	−59.4	±	0	−12.4	±	0.5	−7.7	±	0.3	−6.6
ticlopidine	−24.3	±	0.2	−14.8	±	0.1	−41.9	±	0.3	−7.4	±	0.2	−6.4	±	0.1	−5.8
valerylsalicylate	−12.8	±	0.1	−165.4	±	0.2	−27.4	±	0.8	−157.6	±	1.2	−6.3	±	0.6	−6.0
DFP	−26.8	±	0.2	−36.7	±	0.2	−49.5	±	0.7	−20.8	±	0.2	−3.6	±	0.2	−5.5[c]
L745,337	−28.5	±	0.3	−32.0	±	0.3	−51.1	±	0.1	−19.4	±	0.1	−5.0	±	0.1	−5.5[c]
SC58 125	−28.2	±	0.2	−34.5	±	0.0	−50.3	±	1.2	−29.5	±	0.7	−8.3	±	0.4	−5.5[c]
paracetamol	−12.3	±	0.0	−35.5	±	0.8	−26.0	±	0.2	−26.6	±	0.8	−5.1	±	0.5	−5.5[c]
salicin	−15.2	±	0.1	−68.6	±	0.7	−30.8	±	2.1	−53.2	±	0.7	−4.1	±	0.5	−5.5[c]
salicylaldehyd	−10.6	±	0.0	−19.2	±	0.3	−23.4	±	0.4	−11.1	±	0.4	−5.2	±	0.2	−5.5[c]
sulindac	−21.7	±	0.0	−180.4	±	1.2	−42.1	±	0.3	−166.3	±	1.9	−4.1	±	1.1	−5.5[c]

[a]Calculated according to Scheme 4, see text. [b]Calculated error defined as the standard error of the mean. [c]The value for ΔG_{bind}^{Warner} is approximated to −5.5 kcal/mol from the nondetermined experimental value (IC_{50} > 100 μM).[52]

top scored pose of each docking strategy without any manual intervention and used it as a starting point for MD sampling and rescoring with the LIE method. In all six cases the correlation coefficient for LIE-calculated affinities was poor (r_{LIE} < 0.4), with average unsigned errors unusually high (<|err|> between 5 and 10 kcal/mol). Note that these errors represent underestimation of binding affinities for the majority of compounds, while those with known crystal structures used to initially parametrize γ (Table 1) are all much closer to the ideal correlation line (Supporting Information Figure S2). We could ascribe this unsatisfactory behavior to the fact that many top-scored poses of carboxylated compounds were actually erroneous in the docking protocols used. These ligands are particularly problematic since two binding modes are in principle possible according to crystal structures[63−70] and the docking protocols can assign either pose as the top-ranked depending on the compound, with no consistency within the data set. The first binding mode (Figure 3A) will be referred to herein as the "salt-bridge orientation", since it involves a salt-bridge interaction between the carboxylate group and the positively charged side chain of Arg120. This is the productive orientation for arachidonic acid and the predominant orientation in the crystal structures of COX-1 with different inhibitors. Conversely, the "inverse orientation" (Figure 3D) is

dx.doi.org/10.1021/ci500151f | J. Chem. Inf. Model. 2014, 54, 1488−1499

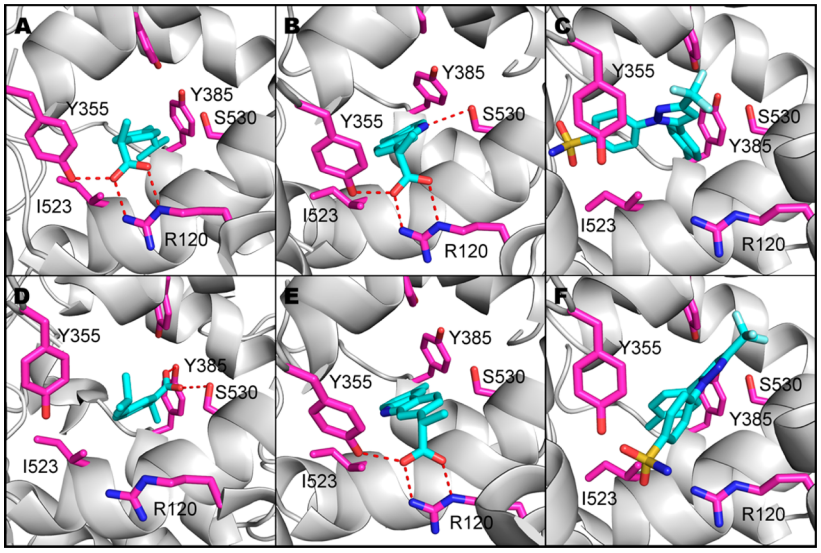

Figure 3. Binding modes of ibuprofen in the salt-bridge (A) and inverse orientation (D). Conformation of carprofen in the salt-bridge orientation with the hydrogen bond interaction with Ser530 present (B) and absent (E). Binding modes of celecoxib where it either occupies the side-pocket (C) or is placed outside of it (F).

defined as the pose where the carboxylate head is oriented toward Ser530 and the opposing Tyr385 found in the entrance of the binding site.

Scheme 2. In order to account for this source of error, we designed Scheme 2 as illustrated in Figure 2. Here, we started from the pool of the four GOLD docking sessions (i.e., using the ASP, ChemScore, GoldScore, and ChemPLP scoring functions). The top-scored pose was now only directly accepted as input for subsequent MD simulations for ligands not belonging to the family of carboxylated compounds or celecoxib analogues. For the latter families of compounds, the poses were instead manually selected among the top ten poses resulting from each scoring function. For carboxylated ligands the salt-bridge interaction (Figure 3A) was the primary selection criterion while hydrogen bond interactions with Ser530 (Figure 3B) were also prioritized if applicable. However, not all carboxylated ligands presented a salt-bridge orientation within the top ten poses for two of the scoring functions considered (Table 2). Further, although it was noted that GlideScore SP was the scoring function that most consistently placed the carboxylated ligands in the salt-bridge orientation (Table 2), it was not possible to use Scheme 2 on the ligands docked with GLIDE as the program cannot be forced to return sufficiently many poses for each ligand. Although all generated poses were examined it was concluded that in the few ligand cases where more than one pose was returned, the top scored pose was consistently in agreement with the poses that would have been manually selected (i.e, the lower scored poses did not offer any improvements in the docking orientation).

For coxibs the side pocket occupancy (behind Tyr355 in Figure 3C) was the primary criterion for selection, which turned out not be fulfilled in any of the top-scored binding modes that were used in Scheme 1 (Figure 3F). The occupancy of this side pocket by coxibs is supported by the crystal structure available of celecoxib in COX-1[71] and coxibs cocrystallized with the COX-2 isoform.[7,72] As expected, the performance of the docking scoring functions (r_{score} in Table 2) did not improve with this knowledge-based selection of docking poses, because the scoring function that was unsuccessful for internal ranking of docking poses is the same as used for the estimation of relative affinities within the series. On the other hand, the average unsigned error and the accuracy of the estimated binding affinities calculated with the LIE method improved slightly (Table 2). Note that in this case the corresponding Pearson correlation coefficients (r_{LIE}) get slightly worse, due to the nature of this coefficient being very sensitive to the spread of the points. GoldScore was the most successful scoring function when it comes to providing starting poses for MD/LIE affinity estimations. Using this scoring function, the binding affinity of 32% of the ligands in Scheme 1 (top scored) and 37% in Scheme 2 (manual selection within top ten) were predicted within an error of 2 kcal/mol using MD/LIE (see Table 2).

Scheme 3. While the results of Scheme 2 are in line with the idea that a careful selection of starting docking poses improves the performance of LIE estimations,[73] the actual selection of docking poses is far from optimal and the estimation of binding affinities is below the accuracy needed in drug design projects (typically, the accepted threshold for <|err|> would be ~1 kcal/mol). Following this line of reasoning, we decided to increase the manual intervention to select initial docking poses for the MD sampling in the LIE method. In Scheme 3, the poses selected from Scheme 2 were thus refined with respect to a set of key interactions that should be attained. All carboxylated ligands were placed in the salt-bridge orientation (Figure 3A) and optimized for hydrogen bond interactions with Ser530 if applicable (Figure 3B). Celecoxib and its analogues were further placed in the side pocket according to the available crystal structure of celecoxib (Figure 3C). Other noncarboxylated ligands were placed in the binding site according to the results from Scheme 2. With this intervention, the average error decreased to 2.1 kcal/mol and Scheme 3 resulted in 63% of all structures reproducing the experimental binding affinities after MD simulations within an error of ±2 kcal/mol, which is a significantly higher percentage than either of the scoring function selected poses from Schemes 1 and 2.

Scheme 4. Finally, we present the most pragmatic scheme, which is herein referred to as Scheme 4 and corresponds to a "pooled data strategy". Here, the LIE calculated affinities

dx.doi.org/10.1021/ci500151f | J. Chem. Inf. Model. 2014, 54, 1488−1499

obtained in each of the three earlier schemes are all considered and only the most negative value for ΔG^{calc}_{bind} is retained for each compound, regardless of the scheme used. Thus, each compound has 11 independent LIE-based predictions associated with it, which originate from 11 different starting poses. These are the top-ranked pose from each of the six scoring functions considered in Scheme 1, the manually selected pose from the four scoring functions selected in Scheme 2, and the refined docking pose considered in Scheme 3. Figure 4

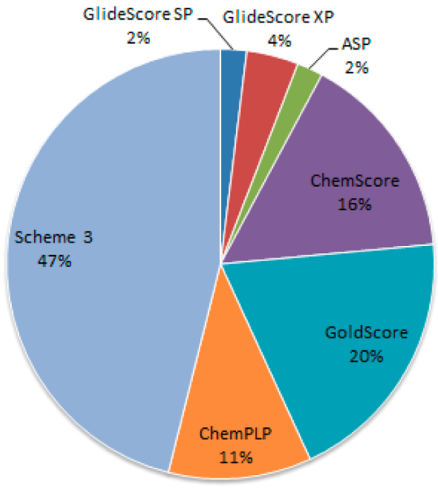

Figure 4. Pie-chart showing the percentage of compounds for which each docking method provided the lowest binding energy estimate used in Scheme 4

illustrates which of the docking schemes generate the most favorable predicted binding free energy (most negative value of ΔG^{calc}_{bind}) for the whole data set. It is readily seen that none of the scoring functions could be considered particularly successful in this respect, and even the most accurate scheme for docking (manual refinement) could only provide the best starting pose for roughly half of the data set. There are two main advantages in using the pooled data strategy of Scheme 4. First, the predictions improve significantly, with the average unsigned error decreasing from 2.1 (Scheme 3) to 1.4 kcal/mol, and with 92% of the ligands being within an error lower than 2 kcal/mol. Second, this strategy provides an optimal combination between user-assessed and automated selection of docking poses. That is, while it considers all strategies for generating docking poses, the final selection of the best pose is solely based on the actual value calculated with LIE, which is then used as a postscoring function. For these reasons, i.e., performance and practical application, Scheme 4 should be considered the optimal strategy to predict binding affinities.

Further analysis of this scheme confirms that none of the scoring functions could be relied upon to provide appropriate starting configurations for all ligands (Figure 4). The average structures of each of the 45 COX-1 ligand complexes selected in this Scheme were generated and analyzed. For the seven compounds that have a crystal structure available in complex with any COX enzyme, a direct comparison is provided in Table 1. In addition, we identified three compounds (6MNA, indometacine, suprofen) whose chemical scaffold is very similar to some of the crystallized compounds[66,68,74] and these were therefore also included in the comparison. Overall, the predicted poses show an excellent superposition with the crystal structure, the only exception being diclofenac, discussed in more detail below. The average RMSD for the remaining six compounds crystallized is 1.3 Å. This value drops even further to 1.1 Å if 6MNA, indometacine, and suprofen are included, by superimposing just the common scaffolds with their respective crystallized analogues.

The case of diclofenac is analyzed in more detail in Figure 5, illustrating further the problem of the dual orientation for

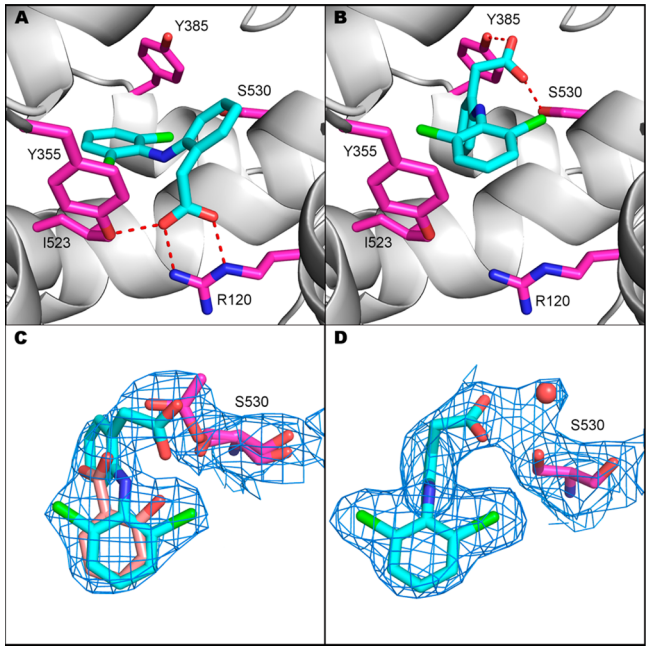

Figure 5. (A) Average MD structure of diclofenac with the lowest calculated binding free energy (Scheme 4) compared to (B) the conformation in the ovine COX-1 crystal structure.[9] (C, D) Calculated $2F_o - F_c$ electron density map (contoured at 1σ) provided by the EDS server[75] together with the diclofenac and salicylate models of the two monomers in the crystal structure.

carboxylated compounds. Figure 5A shows the average structure of the MD simulations corresponding to the salt-bridge orientation, while Figure 5B corresponds to a simulation of the inverse orientation proposed in the crystal structures available for this ligand.[9,63] Our results predict that the salt-bridge orientation is strongly favored in terms of binding free energy (by as much as 12 kcal/mol), but this orientation clearly does not fit the electron density of the available COX-1 crystal structure (PDB code 3N8Y).[9] It should, however, be noted that this relatively low resolution (2.6 Å) experimental structure is not so easy to interpret. The enzyme was incubated with a high concentration of aspirin (10000 times higher than that of diclofenac) and it has strong and continuous electron density between the key binding residue Ser530 and the ligand. This density was modeled in terms of different alternatives for the two protein monomers. In one model, Ser530 was considered to have been acetylated by aspirin and having only partial occupancy by diclofenac (Figure 5C). In the other monomer, diclofenac was modeled with full occupancy together with an additional water molecule (Figure 5D). It is, however, noteworthy that the salicylate model has the ligand in the opposite orientation to that of an earlier structure.[67] The observed density[9] could perhaps also be explained by multiple binding modes of salicylate but, at any rate, it seems indicative of an unusual structure that may not correspond to the actual situation in the binding assay.

dx.doi.org/10.1021/ci500151f | J. Chem. Inf. Model. 2014, 54, 1488−1499

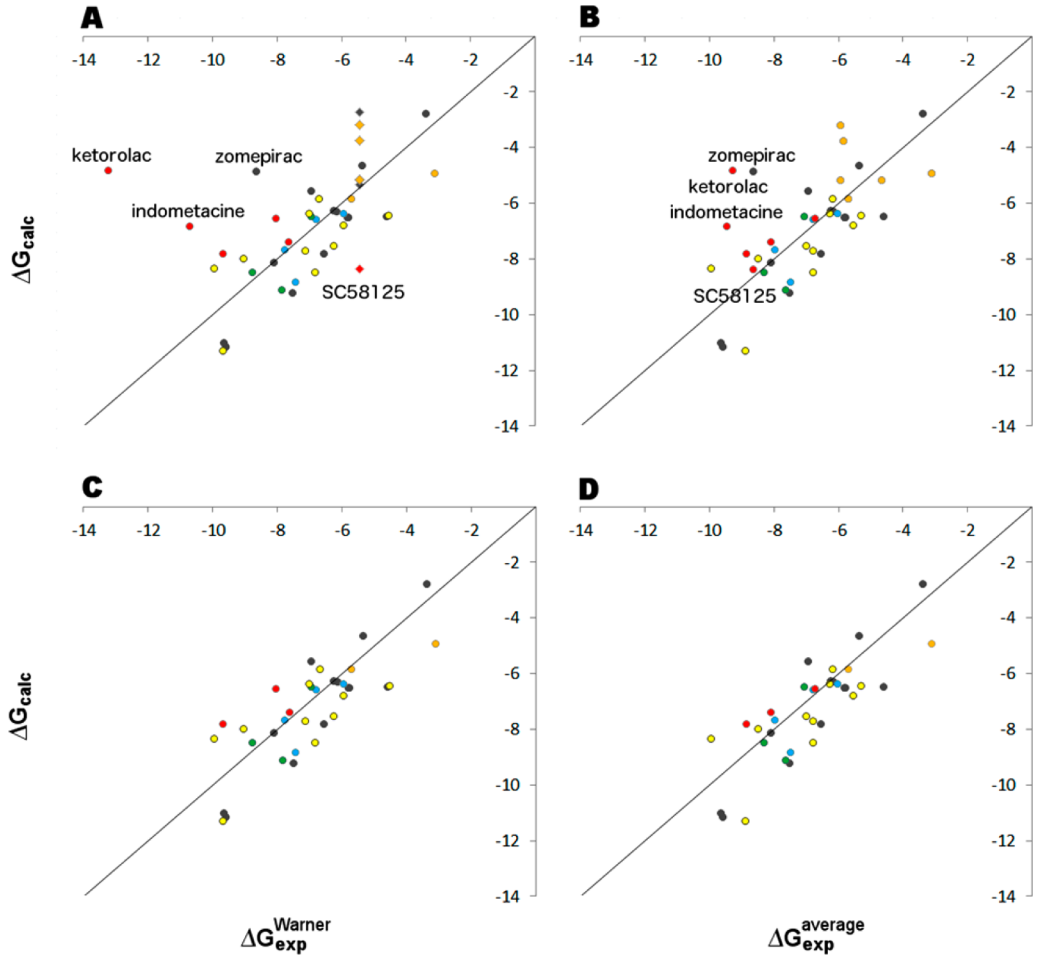

Figure 6. Scatter diagrams of calculated vs experimental binding free energies using the complete Warner data set exclusively (A) and the average of seven data sets (B). Panels C and D show the same data after removal of compounds with undetermined experimental affinity values (IC_{50} > 100 μM, diamonds in panel A) and the three outliers indometacine, ketorolac, and zomepirac (points are color-coded according to the variance of the experimental data (kcal/mol): red > 2 > yellow > 1 > green > 0.5 > blue > 0 = gray and orange = variance unknown).

In support of the above line of reasoning is the fact that our results for the whole subset of carboxylated ligands strongly predict the salt-bridge pose (Figure 3A) to be the most stable, with an average binding free energy difference with respect to the inverse pose (Figure 3D) of −14.8 kcal/mol. The major contribution to this discrimination comes, as expected, from the electrostatic component of the binding free energies. In general, it was found that polar interactions make very important contributions to the binding free energy for carboxylated ligands. Besides the mentioned interactions with the Arg120 and Ser530, additional interactions with water molecules are especially critical for the low binding free energies of carboxylated ligands. In this respect, it is important to sample different water configurations and, in our case, several independent simulations were performed to improve the sampling. The above water interactions were found to be consistently correlated with favorable bidning. For celecoxib and its analogues, on the other hand, the main contribution to the overall binding free energies originates from nonpolar interactions. This is due to the occupancy of the side-pocket (Figure 3C), which is energetically favored as compared to the structures consistently predicted by the docking programs (Figure 3F), where this pocket is empty.

Interestingly, even in the best scheme (Scheme 4) we identified four outliers (Figure 6A). Out of these, indometacine (which was compared to a similar, yet not fully identical crystal structure,[74] see Table 1), zomepirac, and ketorolac all share a common scaffold (Supporting Information Figure S1) and their affinities were consistently underpredicted. A look at the experimental data allows us to identify a source of this bad correlation in terms of the high variability of experimental results for these compounds. There are at least six additional experimental assays on COX-1 available which contain four or more of the ligands reported in the Warner assay.[52] To assess the compatibility of the binding affinities between different data sets they were analyzed with respect to each other. For some of the ligands the variation in experimental affinity is indeed small (Supporting Information Figure S3). However, for indometacine (found in six assays) and ketorolac (found in four assays) the experimental binding affinities span between −5.5 and −11.0 kcal/mol and between −6.1 and −13.2 kcal/mol, respectively.

To further assess the predictive value of our best scheme it is also useful to consider the small subset of seven ligands of the Warner data set which should be considered as nonbinders. These are reported in their study with IC_{50} > 100 μM (corresponding to a threshold of about −5.5 kcal/mol). By fixing the experimental values for these ligands to −5.5 kcal/mol, the MD/LIE scheme can be tested for its ability to separate binders from nonbinders, a rougher estimation as

dx.doi.org/10.1021/ci500151f | J. Chem. Inf. Model. 2014, 54, 1488−1499

compared to the direct comparison with experimental binding affinities. In this case, six out of seven ligands were indeed estimated to have binding free energies more positive than −5.5 kcal/mol. Only SC58125 was overpredicted, (ΔG_{bind}^{calc} = −8.3 kcal/mol). However, as in the case of indometacine and ketorolac above, the variance in experimental data for SC58125 is larger than usual (Figure 6). Hence, better estimates of the experimental affinities for these compounds may be obtained by taking the averages only over measured data points with exact reported values. This yields an average experimental binding free energy of −8.7 kcal/mol for SC58125, which is very close to the calculated one. Indeed, this is in line with the general observation that the correlation between calculations and experiment improves if one takes the *average* experimental values, for ligands with more than one measurement (Figure 6 and Table 2), instead of a *single* experimental value (i.e., the Warner assay).

As seen above, the statistical results of Scheme 4 were improved by comparing the calculated binding free energies to the average experimental ones (Table 2). Naturally, the performance of Schemes 3 and 4 is further improved by removing ketorolac, indometacine, and zomepirac from the data set (Figure 6C, D). For Scheme 4 the average unsigned error decreases to 0.88 kcal/mol, with a calculated r value of 0.81, which indicates a very strong correlation between the calculated and experimental data. The reason for these outlier cases may thus be both uncertainties in experimental affinities and suboptimal docking poses.

CONCLUSIONS

We have presented LIE calculations here for a large and structurally diverse set of traditional NSAIDs and coxibs to COX-1, which has previously been reported as a difficult target for automated molecular docking. Different schemes for obtaining suitable initial poses for MD simulation and LIE scoring have been analyzed and an inescapable conclusion is that automated docking alone is not sufficiently reliable to attain predictive results in this case. This is evidenced by the significant improvement of the results when knowledge-based manual docking is used as a complement to the automated procedures. Our most reliable scheme (Scheme 4) achieves very good performance for this diverse set of inhibitors and is unbiased in the sense that the docking pose with the lowest binding free energy estimated by LIE is the final one chosen, irrespective of by which method it was obtained.

The diversity of the compounds studied here is reflected both by significantly different molecular scaffolds and a mixture of charged and neutral molecules. This situation makes the data set extremely difficult to analyze by rigorous free energy perturbation calculations, since such methods are essentially limited to similar compounds with a common binding mode. Interestingly, the present results once again give strong support to our standard parametrization of the LIE method.[45,46] It is also noteworthy that the simple electrostatic correction term for charged compounds (corresponding to Coulomb's law with an effective dielectric constant of water) clearly improves the results, which corroborates the physical soundness of the model. For example, without including this term the γ obtained by parametrization against only noncarboxylated compounds is −5.9 kcal/mol, while the corresponding value for parametrization agaist only carboxylated ligands without the electrostatic correction is −7.7 kcal/mol. The difference is thus 1.8 kcal/mol, which indicates that the optimal effective dielectric constant in eq 2 is ∼50 (rather than 80 as actually used), which is a very reasonable value for long-range electrostatics in solvated proteins.

Besides the problem of obtaining accurate enough docking poses for binding free energy evaluation by MD simulation, we have also in the case of COX-1 identified incongruent experimental data as a source of error in the comparison with the calculations. This situation is probably not entirely uncommon and may thus plague attempts at accurate affinity prediction. It is, however, encouraging that our results show that optimal performance is attained when the pose with the lowest predicted LIE binding free energy, out of many suggested poses, is picked for the final binding affinity evaluation. This reinforces earlier findings that the methodology is useful for ranking different possible ligand binding modes.[76] The schemes described herein can easily be transferred to other biological systems and we thus expect MD/LIE simulations to provide an efficient way both for ranking ligands and comparing their possible binding orientations for a variety of targets. It also seems that this approach may work better than previously anticipated even for sets of structurally diverse ligands which are usually challenging for standard molecular docking protocols.

ASSOCIATED CONTENT

Supporting Information

Chemical structures and experimental binding affinities of ligands and the complete set of plots of calculated vs experimental binding affinities generated with the all the models reported here. This material is available free of charge via the Internet at http://pubs.acs.org

AUTHOR INFORMATION

Corresponding Author

*Phone: +46 18 471 4109. Fax: +46 18 53 69 71. E-mail: aqvist@xray.bmc.uu.se.

Notes

The authors declare no competing financial interest.

ACKNOWLEDGMENTS

Support from the Swedish Research Council (VR), the eSSENCE e-science initiative and the Swedish National Infrastructure for Computing (SNIC) is gratefully acknowledged. We thank Geir Isaksen for technical assistance in the statistical analyses.

ABBREVIATIONS

MD, molecular dynamics; LIE, Linear Interaction Energy; COX, cyclooxygenase; NSAID, nonsteroidal anti-inflammatory drug

REFERENCES

(1) Melkinova, I. Pain market. *Nat. Rev. Drug Discovery* **2010**, *9*, 589−590.

(2) Wilcox, C. M.; Cryer, B.; Triadafilopoulos, G. Patterns of Use and Public Perception of Over-the-Counter Pain Relievers: Focus on Nonsteroidal Antiinflammatory Drugs. *J. Rheumatol.* **2005**, *32*, 2218−2224.

(3) Winkelmayer, W. C.; Waikar, S. S.; Mogun, H.; Solomon, D. H. Nonselective and cyclooxygenase-2-selective NSAIDs and acute kidney injury. *Am. J. Med.* **2008**, *121*, 1092−1098.

(4) Schneider, V.; Lévesque, L. E.; Zhang, B.; Hutchinson, T.; Brophy, J. M. Association of selective and conventional nonsteroidal

anti-inflammatory drugs with acute renal failure: a population-based, nested case-control analysis. *Am. J. Epidemiol.* **2006**, *164*, 881−889.
(5) Steinmeyer, J. Pharmacological basis for the therapy of pain and inflammation with nonsteroidal anti-inflammatory drugs. *Arthritis Res.* **2000**, *2*, 379−385.
(6) Picot, D.; Loll, P. J.; Garavito, R. M. The X-ray crystal structure of the membrane protein prostaglandin H2 synthase-1. *Nature* **1994**, *367*, 243−249.
(7) Kurumbail, R. G.; Stevens, A. M.; Gierse, J. K.; McDonald, J. J.; Stegeman, R. A.; Pak, J. Y.; Gildehaus, D.; Iyashiro, J. M.; Penning, T. D.; Seibert, K.; Isakson, P. C.; Stallings, W. C. Structural basis for selective inhibition of cyclooxygenase-2 by anti-inflammatory agents. *Nature* **1996**, *384*, 644−648.
(8) Chandrasekharan, N. V.; Dai, H.; Roos, K. L.; Evanson, N. K.; Tomsik, J.; Elton, T. S.; Simmons, D. L. COX-3, a cyclooxygenase-1 variant inhibited by acetaminophen and other analgesic/antipyretic drugs: cloning, structure, and expression. *Proc. Natl. Acad. Sci. U.S.A.* **2002**, *99*, 13926−13931.
(9) Sidhu, R. S.; Lee, J. Y.; Yuan, C.; Smith, W. L. Comparison of Cyclooxygenase-1 Crystal Structures: Cross-Talk between Monomers Comprising Cyclooxygenase-1 Homodimers. *Biochemistry* **2010**, *49*, 7069−7079.
(10) Vane, J. R.; Botting, R. M. Mechanism of action of nonsteroidal anitinflammatory drugs. *Am. J. Med.* **1998**, *104*, 2S−8S.
(11) Bresalier, R. S.; Sandler, R. S.; Quan, H.; Bolognese, J. A.; Oxenius, B.; Horgan, K.; Lines, C.; Riddell, R.; Morton, D.; Lanas, A.; Konstam, M. A.; Baron, J. A. Cardiovascular events associated with rofecoxib in a colorectal adenoma chemoprevention trial. *N. Engl. J. Med.* **2005**, *352*, 1092−102.
(12) Nussmeier, N. A.; Whelton, A. A.; Brown, M. T.; Langford, R. M.; Hoeft, A.; Parlow, J. L.; Boyce, S. W.; Verburg, K. M. Complications of the COX-2 inhibitors parecoxib and valdecoxib after cardiac surgery. *N. Engl. J. Med.* **2005**, *352*, 1081−91.
(13) Solomon, S. D.; McMurray, J. J.; Pfeffer, M. A.; Wittes, J.; Fowler, R.; Finn, P.; Anderson, W. F.; Zauber, A.; Hawk, E.; Bertagnolli, M. Cardiovascular risk associated with celecoxib in a clinical trial for colorectal adenoma prevention. *N. Engl. J. Med.* **2005**, *352*, 1071−80.
(14) Kakuta, H.; Zheng, X.; Oda, H.; Harada, S.; Sugimoto, Y.; Sasaki, K.; Tai, A. Cyclooxygenase-1-Selective Inhibitors Are Attractive Candidates for Analgesics That Do Not Cause Gastric Damage. Design and in Vitro/in Vivo Evaluation of a Benzamide- Type Cyclooxygenase-1 Selective Inhibitor. *J. Med. Chem.* **2008**, *51*, 2400−2411.
(15) Boran, A. D. W.; Iyengar, R. Systems approaches to polypharmacology and drug discovery. *Curr. Opin. Drug Discovery Dev.* **2010**, *13*, 297−309.
(16) Meng, E. C.; Shoichet, B. K.; Kuntz, I. D. Automated docking with grid-based energy evaluation. *J. Comput. Chem.* **1992**, *13*, 505−524.
(17) Huang, Niu.; Shoichet, B. K.; Irwin, J. J. Benchmarking Sets for Molecular Docking. *J. Med. Chem.* **2006**, *49*, 6789−6801.
(18) Lindner, M.; Sippl, W.; Radwan, A. A. Pharmacophore elucidation and Molecular Docking Studies on 5-Phenyl-1-(3-pyridyl)-1*H*-1,2,4-triazole-3-carboxylic Acid Derivatives as COX-2 Inhibitors. *Sci. Pharm.* **2010**, *78*, 195−214.
(19) Viegas, A.; Manso, J.; Corvo, M. C.; Marques, M. M. B.; Cabrita, E. J. Binding of Ibuprofen, Ketorolac, and Diclofenac to COX-1 and COX-2 Studied by Saturation Transfer Difference NMR. *J. Med. Chem.* **2011**, *54*, 8555−8562.
(20) Llorens, O.; Perez, J. J.; Palomer, A.; Mauleon, D. Differential binding mode of diverse cyclooxygenase inhibitors. *J. Mol. Graphics Modell.* **2002**, *20*, 359−371.
(21) Garcia-Nieto, R.; Pérez, C.; Gago, F. Automated docking and molecular dynamics simulations of nimesulide in the cyclooxygenase active site of human prostaglandin-endoperoxide synthase-2 (COX-2). *J. Comput. Aided Mol. Des.* **2000**, *14*, 147−160.
(22) Ermondi, G.; Caron, G.; Lawrence, R.; Longo, D. Docking studies on NSAID/COX-2 isozyme complexes using contact statistics analysis. *J. Comput. Aided Mol. Des.* **2004**, *18*, 683−696.
(23) Wesolowski, S. S.; Jorgensen, W. L. Estimation of Binding Affinities for Celecoxib Analogues with COX-2 via Monte Carlo-Extended Linear Response. *Bioorg. Med. Chem. Lett.* **2002**, *12*, 267−270.
(24) Diaz, L.; Bujons, J.; Delgado, A.; Gutierrez-de-Teran, H.; Åqvist, J. Computational Prediction of Structure-Activity Relationships for the Binding of Aminocyclitols to *β*-Glucocerebrosidase. *J. Chem. Inf. Model.* **2011**, *51*, 601−611.
(25) Hansson, T.; Åqvist, J. Estimation of binding free energies for HIV proteinase inhibitors by molecular dynamics simulations. *Protein Eng.* **1995**, *8*, 1137−1144.
(26) Gutierrez-de-Teran, H.; Nervall, M.; Ersmark, K.; Liu, P.; Janka, L. K.; Dunn, B.; Hallberg, A.; Åqvist, J. Inhibitor Binding to the Plasmepsin IV Aspartic Protease from *Plasmodium falciparum*. *Biochemistry* **2006**, *45*, 10529−10541.
(27) Carlsson, J.; Almlöf, M.; Åqvist, J. Combining docking, molecular dynamics and the linear interaction energy method to predict binding modes and affinities for non-nucleoside inhibitors to HIV-1 reverse transcriptase. *J. Med. Chem.* **2008**, *51*, 2648−2656.
(28) Boukharta, L.; Keränen, H.; Stary-Weinzinger, A.; Wallin, G.; de Groot, B. L.; Åqvist, J. Computer Simulations of Structure-Activity Relationships for hERG Channel Blockers. *Biochemistry* **2011**, *50*, 6146−6156.
(29) Andér, M.; Luzhkov, V. B.; Åqvist, J. Ligand Binding to the Voltage-Gated Kv1.5 Potassium Channel in the Open State-Docking and Computer Simulations of a Homology Model. *Biophys. J.* **2008**, *94*, 820−831.
(30) Gupta, K.; Selinsky, B. S.; Kaub, C. J.; Katz, A. K.; Loll, P. J. The 2.0 A resolution crystal structure of prostaglandin H2 synthase-1: structural insights into an unusual peroxidase. *J. Mol. Biol.* **2004**, *335*, 503−518.
(31) Eswar, N.; Marti-Renom, M. A.; Webb, B.; Madhusudhan, M. S.; Eramian, D.; Shen, M.; Pieper, U.; Sali. A. *Comparative Protein Structure Modeling With MODELLER*; Current Protocols in Bioinformatics; John Wiley & Sons, Inc., 2006; Supplement 15, pp 5.6.1−5.6.30.
(32) Friesner, R. A.; Banks, J. L.; Murphy, R. B.; Halgren, T. A.; Klicic, J. J.; Mainz, D. T.; Repasky, M. R.; Knoll, E. H.; Shelley, M.; Perry, J. K.; Shaw, D. E.; Francis, P.; Shenkin, P. S. Glide: a new approach for rapid, accurate docking and scoring. 1. Method and assessment of docking accuracy. *J. Med. Chem.* **2004**, *47*, 1739−1749.
(33) Verdonk, M. L.; Cole, J. C.; Hartshorn, M. J.; Murray, C. W.; Taylor, R. D. Improved Protein-. Ligand Docking Using GOLD. *Proteins: Struct., Funct., Genet.* **2003**, *52*, 609−623.
(34) *The PyMOL Molecular Graphics System*, Version 1.5.0.4; Schrödinger, LLC, 2000.
(35) *Maestro*, version 9.2.; Schrödinger, LLC: New York, 2011.
(36) *MacroModel*, version 9.9; Schrödinger, LLC, New York, 2011.
(37) Marelius, J.; Kolmodin, K.; Feierberg, I.; Aqvist, J. Q: a molecular dynamics program for free energy calculations and empirical valence bond simulations in biomolecular systems. *J. Mol. Graphics Modell.* **1998**, *16*, 213−225.
(38) Jorgensen, W. L.; Maxwell, D. S.; Tirado-Rives, J. Development and Testing of the OPLS All-Atom Force Field on Conformational Energetics and Properties of Organic Liquids. *J. Am. Chem. Soc.* **1996**, *118*, 11225−11236.
(39) Jorgensen, W. L.; Chandrasekhar, J.; Madura, J. D.; Impey, R. W.; Klein, M. L. Comparison of Simple Potential Functions for Simulating Liquid Water. *J. Chem. Phys.* **1983**, *79*, 926−935.
(40) King, G.; Warshel, A. A surface constrained all-atom solvent model for effective simulations of polar solutions. *J. Chem. Phys.* **1989**, *91*, 3647−3661.
(41) Lee, F. S.; Warshel, A. A Local Reaction Field Method for Fast Evaluation of Long-range Electrostatic Interactions in Molecular Simulations. *J. Chem. Phys.* **1992**, *97*, 3100−3107.

(42) Ryckaert, J. P.; Ciccotti, G.; Berendsen, H. J. C. Numerical Integration of the Cartesian equations of motion of a system with constraints: Molecular dynamics of *n*-alkanes. *J. Comput. Phys.* **1977**, *23*, 327−341.
(43) Bjelic, S.; Brandsdal, B. O.; Åqvist, J. Cold Adaptation of Enzyme Reaction. *Biochemistry* **2008**, *47*, 10049−10057.
(44) Åqvist, J.; Medina, C.; Samuelsson, J. E. A new method for predicting binding affinitiy in computer-aided drug design. *Protein Eng.* **1994**, *7*, 385−391.
(45) Hansson, T.; Marelius, J.; Åqvist, J. Ligand binding affinity prediction by linear interaction energy methods. *J. Comput. Aided Mol. Des.* **1998**, *12*, 27−35.
(46) Almlöf, M.; Carlsson, J.; Aqvist, J. Improving the accuracy of the linear interaction energy method for solvation free energies. *J. Chem. Theory Comput.* **2007**, *3*, 2162−2175.
(47) Almlöf, M.; Brandsdal, B. O.; Åqvist, J. Binding Affinity Prediction with Different Force Fields: Examination of the Linear Interaction Energy Method. *J. Comput. Chem.* **2004**, *25*, 1242−1254.
(48) Marelius, J.; Hansson, T.; Åqvist, J. Calculation of ligand binding free energies from molecular dynamics simulations. *Int. J. Quantum Chem.* **1998**, *69*, 77−88.
(49) Cheng, Y.; Prusoff, W. H. Relationship between the inhibitor constant (Ki) and the concentration of inhibitor which causes 50% inhibition (I50) of an enzymatic reaction. *Biochem. Pharmacol.* **1973**, *22*, 3099−3108.
(50) Rogers, D.; Hahn, M. Extended-Connectivity Fingerprints. *J. Chem. Inf. Model.* **2010**, *50*, 742−754.
(51) *JChem*, version 5.10.4; ChemAxon, 2012; http://www.chemaxon.com.
(52) Warner, T. D.; Giuliano, F.; Vojnovic, I.; Bukasa, A.; Mitchell, J. A.; Vane, J. R. Nonsteroid drug selectivities for cyclo-oxygenase-1 rather than cyclo-oxygenase-2 are associated with human gastrointestinal toxicity: A full ***in vitro*** analysis. *Proc. Natl. Acad. Sci. U.S.A.* **1999**, *96*, 7563−7568.
(53) Adams, S. S.; Bresloff, P.; Mason, C. G. Pharmacological differences between the optical isomers of ibuprofen: evidence for metabolic inversion of the (−)-isomer. *J. Pharm. Pharmacol.* **1976**, *28*, 256−257.
(54) Hutt, A. J.; Caldwell, J. The Metabolic chiral inversion of 2-arylpropionic acids. A novel route with pharmacological consequences. *J. Pharm. Pharmacol.* **1983**, *35*, 693−704.
(55) Knihinicki, R. D.; Williams, K. M.; Day, R. O. Chiral inversion of 2-arylpropionic acid non-steroidal anti-inflammatory drugs–1. In vitro studies of ibuprofen and flurbiprofen. *Biochem. Pharmacol.* **1989**, *38*, 4389−95.
(56) Mitchell, J. A.; Akarasereenont, P.; Thiemermann, C.; Flower, R. J.; Vane, J. R. Selectivity of nonsteroidal antiinflammatory drugs as inhibitors of constitutive and inducible cyclooxygenase. *Proc. Natl. Acad. Sci. U.S.A.* **1993**, *90*, 11693−11697.
(57) Patrignani, P.; Panara, M. R.; Greco, A.; Fusco, O.; Natoli, C.; Iacobelli, S.; Cipollone, F.; Ganci, A.; Créminon, C.; Maclouf, J. Biochemical and pharmacological characterization of the cyclooxygenase activity of human blood prostaglandin endoperoxide synthases. *J. Pharmacol. Exp. Ther.* **1994**, *271*, 1705−1712.
(58) Laneuville, O.; Breuer, D. K.; Dewitt, D. L.; Hla, T.; Funk, C. D.; Smith, W. L. Differential inhibition of human prostaglandin endoperoxide H synthases-1 and −2 by nonsteroidal anti-inflammatory drugs. *J. Pharmacol. Exp. Ther.* **1994**, *271*, 927−934.
(59) Brideau, C.; Kargman, S.; Liu, S.; Dallob, A. L.; Ehrich, E. W.; Rodger, I. W.; Chan, C. C. A human whole blood assay for clinical evaluation of biochemical efficacy of cyclooxygenase inhibitors. *Inflamm. Res.* **1996**, *45*, 68−74.
(60) Cryer, B.; Feldman, M. Cyclooxygenase-1 and cyclooxygenase-2 selectivity of widely used nonsteroidal anti-inflammatory drugs. *Am. J. Med.* **1998**, *104*, 413−421.
(61) Kato, M.; Nishida, S.; Kitasato, H.; Sakata, N.; Kawai, S. Cyclooxygenase-1 and cyclooxygenase-2 selectivity of non-steroidal anti-inflammatory drugs: investigation using human peripheral monocytes. *J. Pharm. Pharmacol.* **2001**, *53*, 1679−1685.
(62) Mishra, S. K.; Sund, J.; Åqvist, J.; Koča, J. Computational Prediction of Monosaccharide Binding Free Energies to Lectins with Linear Interaction Energy Models. *J. Comput. Chem.* **2012**, *33*, 2340−2350.
(63) Rowlinson, S. W.; Kiefer, J. R.; Prusakiewicz, J. J.; Pawlitz, J. L.; Kozak, K. R.; Kalgutkar, A. S.; Stallings, W. C.; Kurumbail, R. G.; Marnett, L. J. A novel mechanism of cyclooxygenase-2 inhibition involving interactions with Ser-530 and Tyr-385. *J. Biol. Chem.* **2003**, *278*, 45763−45769.
(64) Gupta, K.; Selinsky, B. S.; Loll, P. J. 2.0 angstroms structure of prostaglandin H2 synthase-1 reconstituted with a manganese porphyrin cofactor. *Acta Crystallogr.,Sect.D* **2006**, *62*, 151−156.
(65) Selinsky, B. S.; Gupta, K.; Sharkey, C. T.; Loll, P. J. Structural analysis of NSAID binding by prostaglandin H2 synthase: time-dependent and time-independent inhibitors elicit identical enzyme conformations. *Biochemistry* **2001**, *40*, 5172−5180.
(66) Duggan, K. C.; Walters, M. J.; Musee, J.; Harp, J. M.; Kiefer, J. R.; Oates, J. A.; Marnett, L. J. Molecular basis for cyclooxygenase inhibition by the non-steroidal anti-inflammatory drug naproxen. *J. Biol. Chem.* **2010**, *285*, 34950−34959.
(67) Loll, P. J.; Picot, D.; Garavito, R. M. The structural basis of aspirin activity inferred from the crystal structure of inactivated prostaglandin H2 synthase. *Nat. Struct. Biol.* **1995**, *2*, 637−643.
(68) Loll, P. J.; Picot, D.; Ekabo, O.; Garavito, R. M. Synthesis and use of iodinated nonsteroidal antiinflammatory drug analogs as crystallographic probes of the prostaglandin H2 synthase cyclooxygenase active site. *Biochemistry* **1996**, *35*, 7330−7340.
(69) Malkowski, M. G.; Ginell, S. L.; Smith, W. L.; Garavito, R. M. The Productive Conformation of Arachidonic Acid Bound to Prostaglandin Synthase. *Science* **2000**, *289*, 1933−1937.
(70) Kiefer, J. R.; Pawlitz, J. L.; Moreland, K.t.; Stegeman, R. A.; Hood, W. F.; Gierse, J. K.; Stevens, A. M.; Goodwin, D. C.; Rowlinson, S. W.; Marnett, L. J.; Stallings, W. C.; Kurumbail, R. G. Structural insights into the stereochemistry of the cyclooxygenase reaction. *Nature* **2000**, *405*, 97−101.
(71) Rimon, G.; Sidhu, R. S.; Lauver, D. A.; Lee, J. Y.; Sharma, N. P.; Yuan, C.; Frieler, R. A.; Trievel, R. C.; Lucchesi, B. R.; Smith, W. L. Coxibs interfere with the action of aspirin by binding tightly to one monomer of cyclooxygenase-1. *Proc. Natl. Acad. Sci. U.S.A.* **2010**, *107*, 28−33.
(72) Wang, J. L.; Limburg, D.; Graneto, M. J.; Springer, J.; Hamper, J. R.; Liao, S.; Pawlitz, J. L.; Kurumbail, R. G.; Maziasz, T.; Talley, J. J.; Kiefer, J. R.; Carter, J. The Novel benzopyran class of selective cyclooxygenase-2 inhibitors. Part 2: the second clinical candidate having a shorter and favorable human half-life. *Bioorg. Med. Chem. Lett.* **2010**, *20*, 7159−7163.
(73) Bjelic, S.; Nervall, M.; Gutiérrez-de-Teràn, H.; Ersmark, K.; Hallberg, A.; Åqvist, J. Computational inhibitor design against malaria plasmepsins. *Cell. Mol. Life. Sci.* **2007**, *64*, 2285−2305.
(74) Harman, C. A.; Turman, M. V.; Kozak, K. R.; Marnett, L. J.; Smith, W. L.; Garavito, R. M. Structural Basis of enantioselective Inhibition of Cyclooxygenase-1 by S-α-Substituted Indomethacin Ethanolamides. *J. Biol. Chem.* **2007**, *282*, 28096−28105.
(75) Kleywegt, G. J.; Harris, M. R.; Zou, J. Y.; Taylor, T. C.; Wählby, A.; Jones, T. A. The Uppsala Electron-Density Server. *Acta Crystallogr.* **2004**, *D60*, 2240−2249.
(76) Nervall, M.; Hanspers, P.; Carlsson, J.; Boukharta, L.; Åqvist, J. Predicting binding modes from free energy calculations. *J. Med. Chem.* **2008**, *51*, 2657−2667.